Microsyst Technol (2017) 23:3215–3225
DOI 10.1007/s00542-016-3015-z

TECHNICAL PAPER

Capacitive MEMS absolute pressure sensor using a modified commercial microfabrication process

Adel Merdassi[1] · Charles Allan[2] · Edward J. Harvey[3] · Vamsy P. Chodavarapu[4]

Received: 1 June 2016 / Accepted: 5 June 2016 / Published online: 20 June 2016
© Springer-Verlag Berlin Heidelberg 2016

Abstract We present the design and fabrication of a capacitive absolute pressure sensor using a modified commercial microfabrication process. The pressure sensor is fabricated using MEMS Integrated Design for Inertial Sensors (MIDIS), a process recently developed by Teledyne DALSA Semiconductor Inc. (TDSI). The MIDIS process provides wafer-level vacuum encapsulation under a high vacuum pressure of 10 mtorr, which enables the absolute pressure measurement. We perform post-fabrication processing of the obtained devices from the foundry to create a thin single crystal silicon membrane and expose it to atmospheric pressure to serve as the sensing membrane for the pressure sensor. The proposed pressure device includes Through Silicon Vias (TSVs) suitable for flip-chip bonding with a signal conditioning integrated circuit. The presented sensor uses a deflectable large membrane with accurate controllable thickness and offers a high sensitivity of 16.5 fF/kPa with a good linearity over designed pressure range of 101–125 kPa. The operating pressure range can be modified by simply varying the physical dimensions of the sensing membrane. We demonstrate several prototype absolute capacitive pressure sensors with different membrane diameters ranging from 140 to 360 μm and thicknesses ranging from 1 to 10 μm with a fixed gap of 2 μm between the membrane and immovable electrode. The sensor calibration data is collected in a regulated pressure chamber using a reference commercial pressure sensor.

✉ Vamsy P. Chodavarapu
vchodavarapu1@udayton.edu

Adel Merdassi
adel.merdassi@mail.mcgill.ca

Charles Allan
charles.allan@nxtsens.com

Edward J. Harvey
edward.harvey@mcgill.ca

[1] Department of Electrical and Computer Engineering, McGill University, 3480 University Street, Montreal, QC H3A 0E9, Canada

[2] Nxtsens Microsystems Inc., 1000 de La Gauchetière Ouest, 43rd Floor, Montreal, QC H3B 4W5, Canada

[3] Division of Orthopaedic Surgery, McGill University, 1650 Cedar Avenue, Montreal, QC H3G 1A4, Canada

[4] Department of Electrical and Computer Engineering, University of Dayton, 300 College Park, Dayton, OH 45469, USA

1 Introduction

Micro-Electro-Mechanical Systems (MEMS) pressure sensors are widely used in a variety of industrial, consumer electronics and medical applications due to their small size, low cost and low power consumption (Wise 2007). Examples of applications include automotive and aerospace systems (engine manifold, tires, braking system, etc.) (Fleming 2001; Leclerc 2007), consumer applications (wearable, gaming devices, smartphones, etc.) (Lee et al. 2015; Hsu and Young 2014), medical applications (intraocular, intracranial and arterial pressure measurement and blood pressure measurement, etc.) (Chitnis et al. 2013; Chiou et al. 2016; Chan et al. 2014). The volume and market value of MEMS pressure sensors sold each year is the highest among the MEMS devices and grew at Compound Annual Growth Rate (CAGR) of 9.7 % from 2010 to 2015 ($1.94 Billion US) (Bryzek et al. 2006). According to TechNavio's analysts (PRNewswire 2015), the growth prospects of the global MEMS Pressure Sensors market will reach a CAGR of 9.1 % over the period

2015–2019. Majority of the growth in the MEMS pressure sensors is being driven by smartphones and wearable devices where 10 degree-of-freedom inertial measurement units are now being widely used that consist of a 3-axis accelerometer, 3-axis gyroscope, 3-axis magnetometer and a pressure sensor (for altitude measurement) (Mounier and Girardin 2015). Thus, there is a tremendous interest to develop MEMS pressure sensors in the same microfabrication process that allows development of inertial sensors like accelerometers and gyroscopes, as described in the current work.

The Quality factor (Q) of a vibratory micromechanical structure is impacted by many different damping mechanisms include anchor loss, thermoelastic dissipation, surface loss, and air damping (Sharma et al. 2012). Vibratory MEMS inertial sensors require a good quality ultra-clean hermetic encapsulation with low leakage to help achieve a high Q and maintain stability of the Q for long-term operation (Choa 2005). Currently, the MEMS Integrated Design for Inertial Sensors (MIDIS) process, introduced by Teledyne DALSA Semiconductor Inc. (TDSI) in 2013, is the world's only pure-play commercial microfabrication process with ultra-clean wafer-level vacuum encapsulation needed for high Q inertial sensor development (Esashi 2008). MIDIS is a high aspect ratio bulk micromachining process of a 30 µm thick Single Crystal Silicon (SCS) device layer that is sandwiched between two silicon wafers, a bottom handle wafer and top interconnect wafer. The device layer is vacuum encapsulated at the vacuum pressure of 10 mtorr. The total leak rate equivalent in MIDIS process varies from one fabrication run to another between 6.3×10^{-13} and 6.5×10^{-17} atm cm^3/s (Merdassi et al. 2015a). Using MIDIS, we have previously developed a variety of MEMS devices including inertial sensors and timing devices (Merdassi et al. 2015a, b; Xereas and Chodavarapu 2015). In the current work, we present the design, fabrication and testing of a pressure sensor fabricated using MIDIS process. We perform post-fabrication processing of the obtained devices from the TDSI foundry to create a thin single crystal silicon membrane and expose it to atmospheric pressure to serve as the sensing membrane for the absolute capacitive pressure sensor.

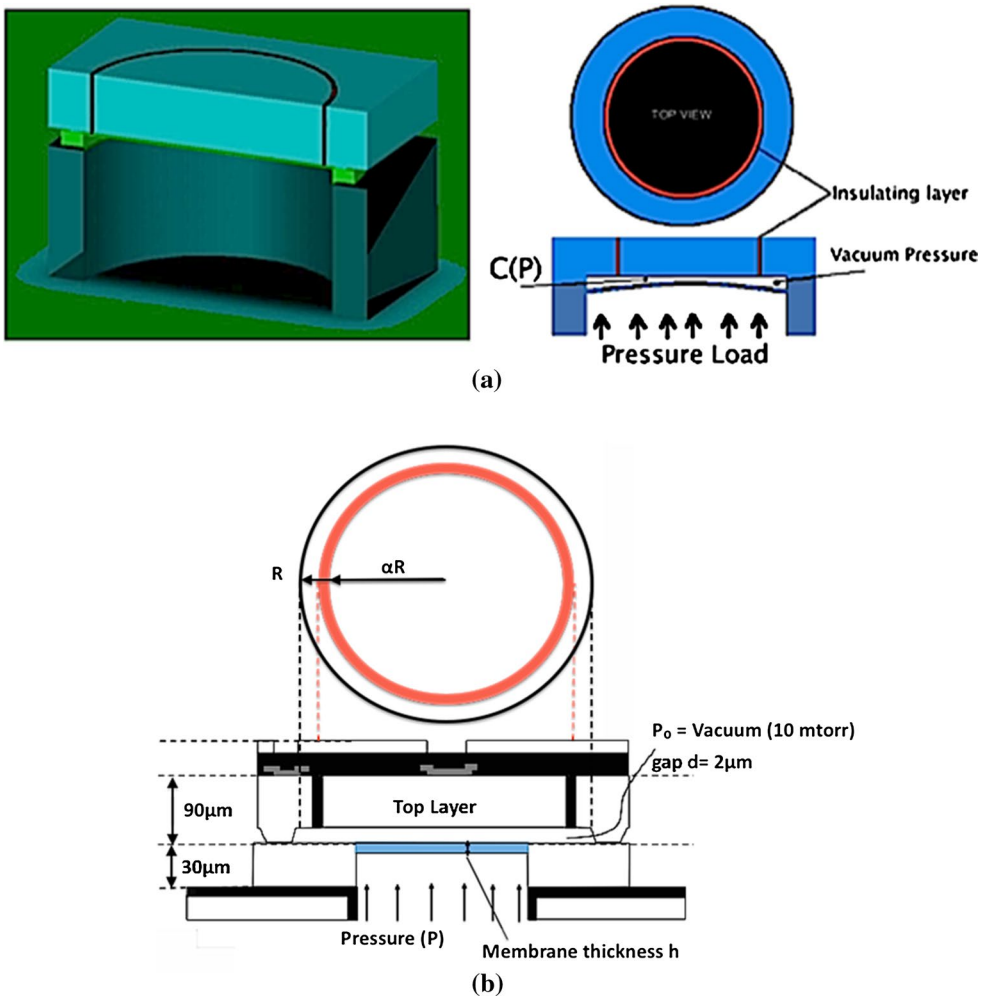

Fig. 1 **a** Cross-sectional view of the 3D model of the pressure sensor. **b** Schematic drawing of the pressure sensor

Pressure sensors are based on various electro-mechanical properties including piezoelectricity, piezoresistivity and capacitance (Barlian et al. 2009; Tadigadapa and Mateti 2009). Capacitive MEMS pressure sensors are preferred in most of the previously listed applications due to their many advantages including good reliability, accuracy and sensitivity, low temperature coefficient, low drift, and low power consumption. Further, the capacitive sensing approach offers a larger dynamic signal response at the output than with using a piezo-resistive transducer. It is important to note that the choice of the microfabrication technology to develop the pressure sensor plays a crucial role to improve the metrology performance, reliability, and allow efficient integration of the MEMS pressure sensor with its readout circuit (Chavan and Wise 2001). Capacitive MEMS pressure sensors typically consist of two parallel plate electrodes. One electrode is able to deflect upon exposure to ambient pressure, while the other is immovable. For absolute sensing applications, there is a known pressure between the parallel plates. The difference in pressure on both sides of the flexible membrane, causes a gradient which leads to a deflection of the membrane. Capacitive MEMS pressure sensors are excellent at detecting pressure changes over a small deflection range and these types of devices are robust and their operation is well understood.

In MEMS absolute pressure sensors, the main challenge comes with creating a vacuum or a reference pressure between the parallel plates. Many micromachining technologies including bulk (dry and wet) and surface micromachining have been used to make the circular and square shapes for the membrane used in the pressure sensors (Kaajakari 2009). Bulk micromachining uses isotropic/anisotropic-wet etching, and eventually, dopant concentration dependent etch stops to control the membrane thickness. However, this method suffers from lack of precise etching control and the dopant concentration dependent etch stop process is sensitive to temperature variations. The alternative is based on using surface micromachining to make a etch hole in a top structural layer and using an isotropic wet etch to remove the sacrificial material between the top structural layer and the bottom electrode material. This releases the top structural layer to create the moveable membrane. In the final step, the etch hole is sealed with a nitride or similar plug (Stone et al. 2010). This approach induces unreliability in the device fabrication yield and non-linearity in the membrane deflection due to the nitride or similar material plug. Further, polycrystalline and amorphous materials used in the sensing membrane for capacitive sensors leads to poor repeatability in the pressure measurement compared to single crystalline material such as SCS (Saejok et al. 2008; Guckel et al. 1988).

In this context, MIDIS process offers extraordinary features in accordance with the specifications needed for high performance, cost-effective and mass-producible MEMS pressure sensors. The device layer available in MIDIS is SCS. MIDIS include ultra-low leak rate high vacuum between the device wafer and the top interconnect wafer required towards absolute pressure sensor development. Finally, MIDIS also includes the ability to monolithically integrate inertial sensors. We perform simulation analysis using both lumped modeling by Architect module and Finite Element Method (FEM) through Coventorware. Currently, the pressure sensor is designed to operate over a range of 101–125 kPa, but the operating pressure range can be changed by suitably designing the thickness of the sensing membrane for specific applications. The pressure sensor is interfaced to a capacitance-to-digital converter circuit from Analog Devices Inc. (Model AD7152). The AD7152 provides good performance in terms of low noise and direct I^2C interface to a microcontroller. The conditioning circuit employs a 12-bit 2-channel Σ-Δ capacitance-to-digital

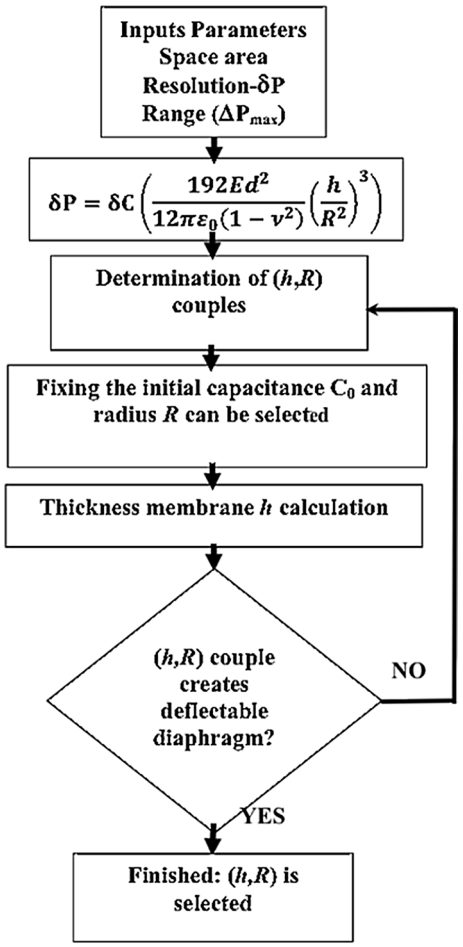

Fig. 2 Flow chart of the design methodology applied to the pressure sensor development

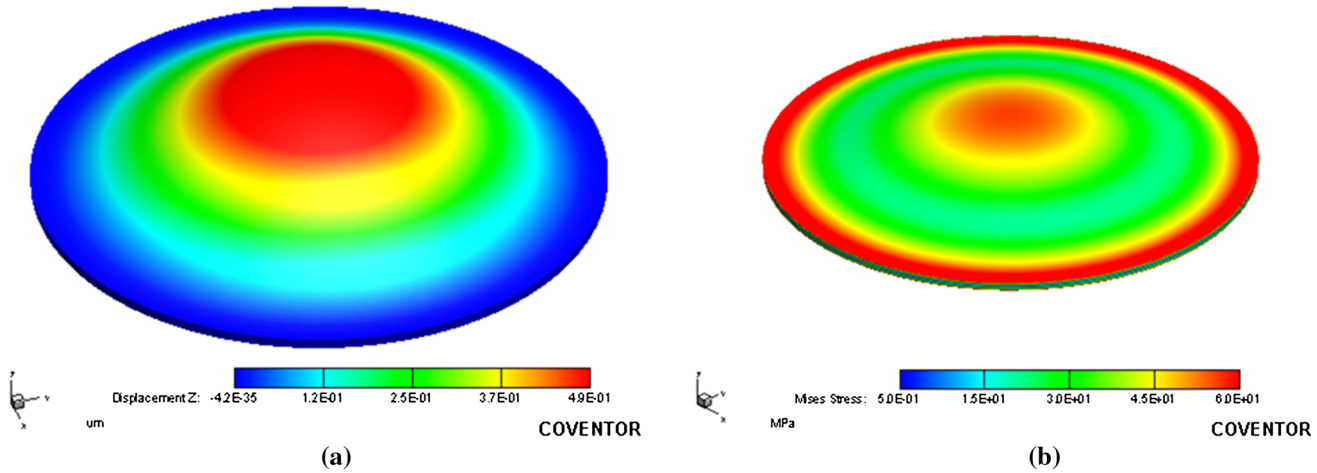

Fig. 3 Micromechanical analysis. **a** Maximum displacement under full pressure range measurement. **b** Mises stress results under the maximum pressure load

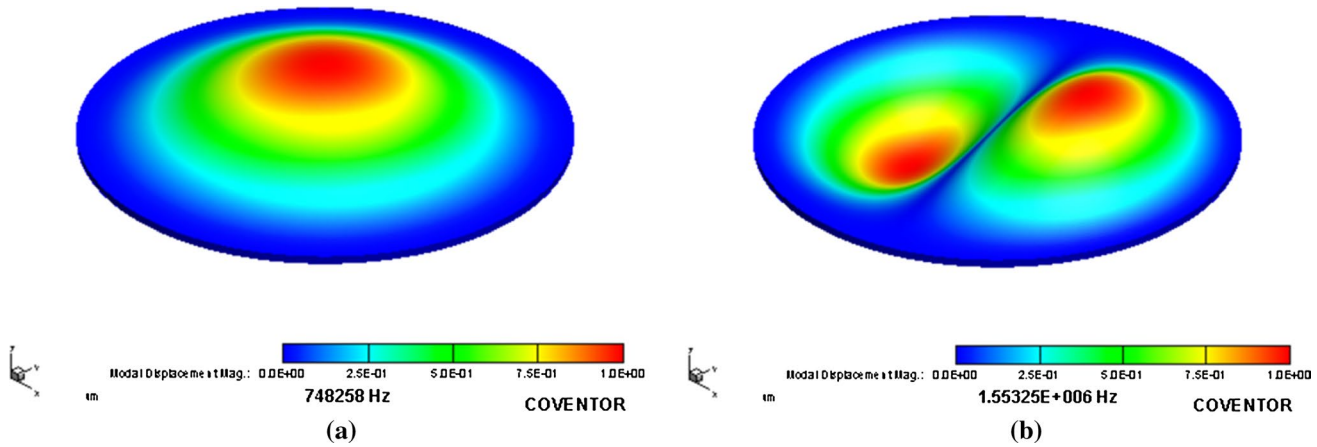

Fig. 4 Modal analysis of the sensing membrane. **a** Fundamental mode. **b** Secondary mode

convertor that offers excellent immunity from the electrical noise, which enhances the sensor resolution.

2 Pressure sensor design and simulation results

The described pressure sensor consists of two electrodes, one of which represents the sensing membrane that undergoes deflection upon the external applied pressure load that is uniformly distributed over the top surface of the membrane. Figure 1a shows the cross-sectional view of 3D model of the proposed sensor. Figure 1b shows the schematic drawing of the pressure sensor. Here, the reference pressure is a high vacuum pressure of 10 mtorr. We chose a circular shape for the membrane which offers low stress behavior than a square shape counterpart. The displacement of the membrane center is linearly proportional to the pressure load. This deformation is then converted into electrical capacitance that will be linearized in order to get a linear relationship between the applied pressure and the output signal.

The displacement at the center of the membrane is given by Eq. (1) (Eaton and Smith 1997b) as,

$$u_0 = u(r = 0) = \frac{R^4}{64D}(P - P_0), \tag{1}$$

where, D is the flexural rigidity, R is the circular membrane radius, P_0 the reference pressure and u_0 the displacement at the center of the membrane. The sensor capacitance can be deduced as (DeHennis and Chae 2008; Jones and Nenadic 2013),

$$C = \int_0^{2\pi} \int_0^{\alpha R} \frac{\varepsilon_0 \varepsilon_r r dr}{d - w(r)} \tag{2}$$

$$C \approx C_0\left[1+\left(1-\alpha^2+\frac{\alpha^3}{3}\right)\frac{u_0}{d}\right] \quad (3)$$

where, α represents the dimensionless ratio that controls the effective radius of the top electrode, d is the gap between the two electrodes, u_0 the displacement at the center of the membrane, r the radius, ε_r the relative permittivity and ε_0 is the permittivity of vacuum.

Finally, based on small deflection mode, where $\mu_o < h$, the sensor sensitivity, S, is given by Eq. (4) as,

$$S = \frac{\partial C}{\partial P} = \frac{\partial C}{\partial u_0}\frac{\partial u_0}{\partial P} = C_0\frac{\left(1-\alpha^2+\frac{\alpha^3}{3}\right)}{d}\frac{R^4}{64D} \quad (4)$$

where, α represents the dimensionless ratio that controls the effective radius of the top electrode, d is the gap between the two electrodes, u_0 the displacement at the center of the membrane, R the membrane radius, D is the flexural rigidity and h the membrane thickness.

The methodology of the design process consists of synthesizing the different dimensional parameters as well as the number of the units constituting the membranes. The intended design aims to find the optimal radius, R, membrane thickness, h, and the acceptable number of units for a compact design with high sensitivity over the design operation pressure range (e.g., 101–125 kPa range in the present case). Figure 2 illustrates the methodology adopted to deduce h, R, and the number of sensing membranes needed for the intended design towards the desired operational range, for example, from atmosphere pressure (101 kPa) to 125 kPa in the current work. Again, the operating pressure range can be changed for different applications by changing the membrane physical dimensions. The FEM method is used to simulate the mechanical parameters characterizing the deflectable membrane. Based on the theoretical calculations, the circular membrane is built with adequate extruded meshing elements. Figure 3a shows the maximum deflection at the center of the membrane and Fig. 3b shows the generated Mises stresses at the clamped regions.

The dynamic performance is characterized by the frequency range over which we can apply a dynamic pressure. This performance is quantified by the fundamental mode that is illustrated by Fig. 4a and the secondary mode is shown in Fig. 4b. Figure 5 illustrates the maximum displacement versus the applied pressure for a given membrane characterized by 5 μm thickness and diameter dimension of 360 μm. The mechanical sensitivity is then deduced from the slope of the curve.

The lumped modeling aims to deduce the sensor sensitivity. Figure 6a shows the maximum displacement of the

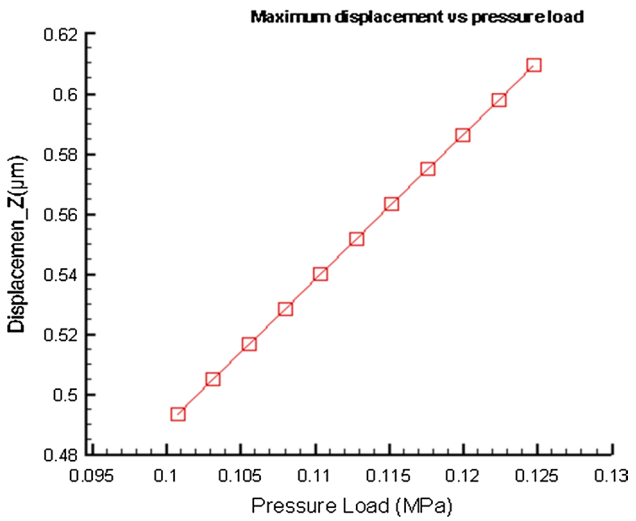

Fig. 5 Maximum displacement of the membrane versus applied pressure load

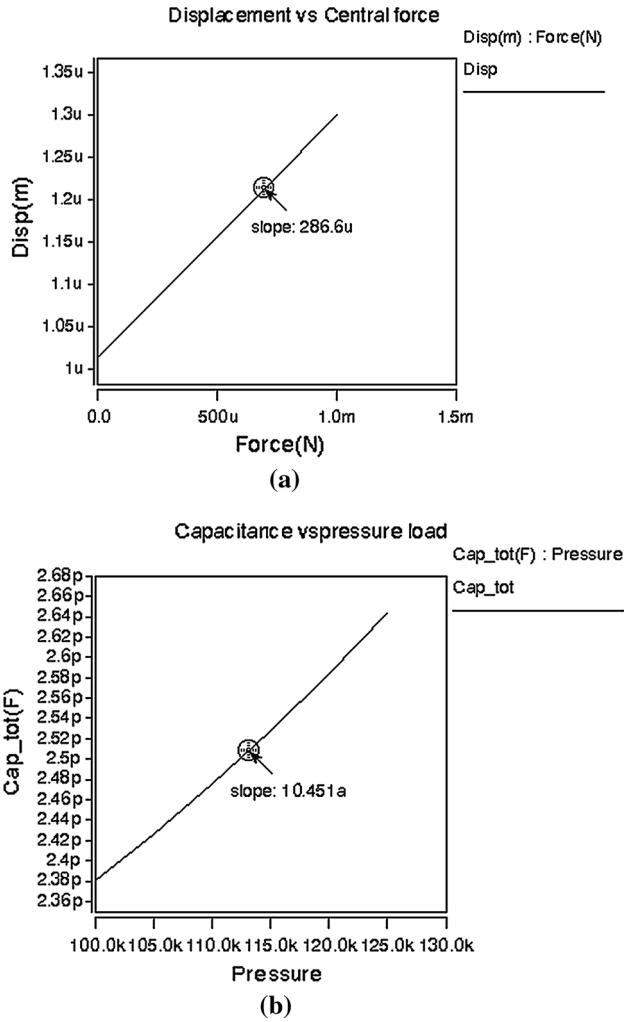

Fig. 6 Coventor architect results. **a** Displacement of the center of the membrane under the application of a vertical force. **b** Capacitance output response as under the application of the applied pressure

central position under the application of a vertical force at the center of the membrane. The slope result is evaluated to 286.6 μm/N. Figure 6b allows the determination of the sensor sensitivity through the calculation of the curve slope. The sensor sensitivity is evaluated to 10 fF/kPa over the current sensor operating range of 101–125 kPa.

3 Fabrication

The pressure sensor is fabricated in two phases. In the first phase, the vacuum encapsulated sandwich structure that consists of the 30 μm thick SCS device wafer placed in between the top interconnect wafer and the bottom handle wafer is fabricated using the standard MIDIS process from TDSI. The gap between the device wafer and the top interconnect wafer is 2 μm which forms the capacitance gap for the pressure sensor. In the second phase, we perform post-fabrication processing of the devices obtained from the TDSI foundry to etch the handle wafer and then selectively etch the device wafer to a desired thickness using Deep Reactive Ion Etching process (DRIE) to form the pressure sensing membrane.

The MIDIS platform is a high aspect ratio bulk micromachining process and its process steps are described in our previous publications (Merdassi et al. 2015a, b; Xereas and Chodavarapu 2015). The handle wafer has a thickness of 380 μm. The interconnect wafer has a thickness of 108 μm. The interconnect wafer includes Through-Silicon Vias (TSVs) to create electrically isolated connections to the device wafer. The process begins by patterning the handle wafer using DRIE to create 30 μm deep silicon cavities in the handle wafer. The pressure sensor is fabricated over this cavity. The surface is then protected by a 1.1 μm thermally grown layer of silicon oxide. The silicon oxide is used to provide electrical isolation to the MEMS device. Next, the device wafer is fusion bonded onto the handle wafer. The interconnect wafer with the TSVs is then fusion bonded to the device wafer. The vacuum cavity for the pressure sensor is based on silicon-on-silicon bonding

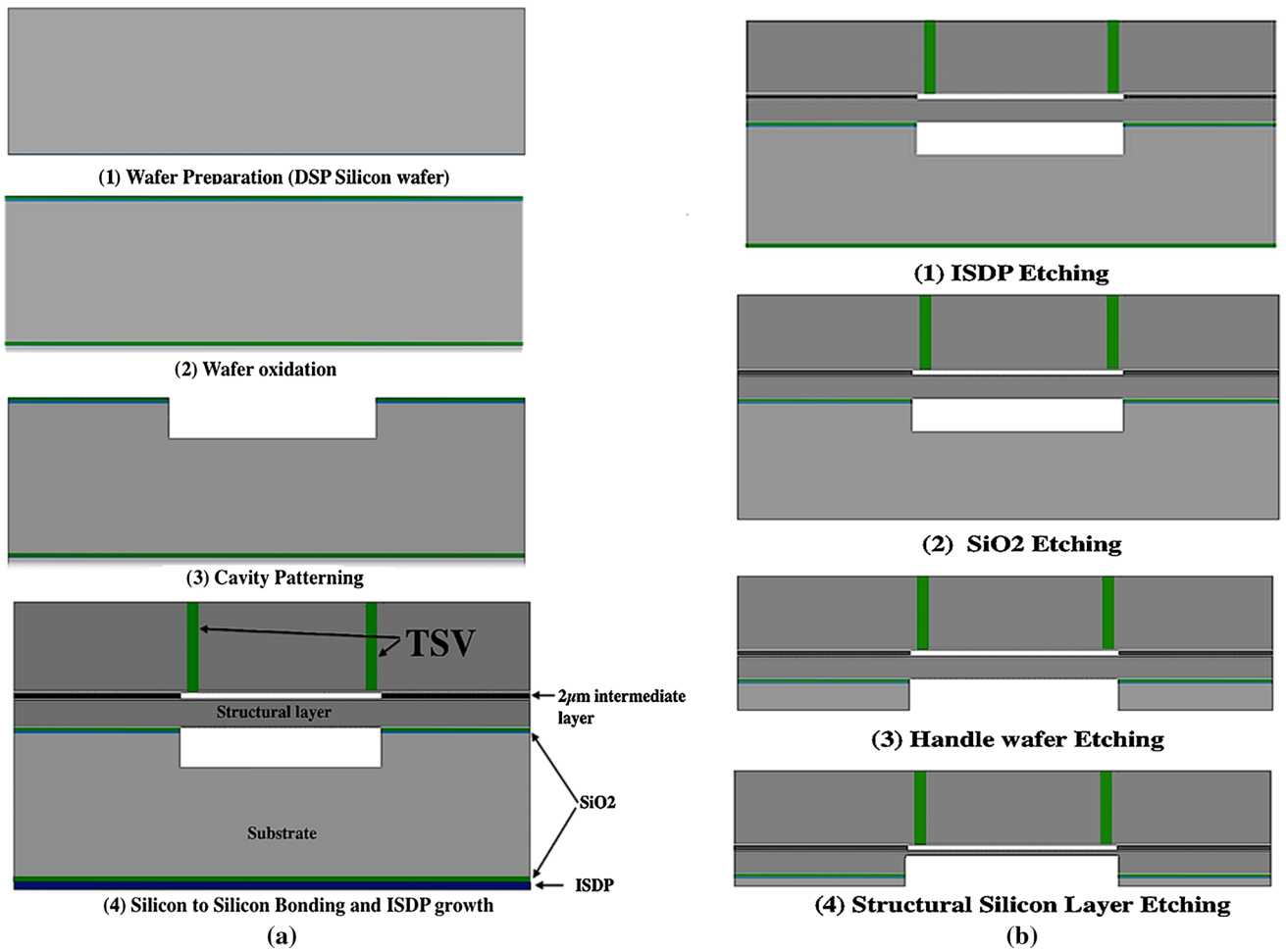

Fig. 7 **a** The main steps constituting the unmodified commercial MIDIS process and **b** post processing Steps completing the sensor fabrication

(or fusion bonding) process that helps to eliminate the effect of thermal mismatch that exist between two different materials. Figure 7a illustrates the important steps involved in the standard MIDIS process.

The second phase consists of post-processing of the fabricated MEMS device obtained from the TDSI foundry to create and expose the thin deflectable membrane. The post-fabrication process steps were created to allow creation of a monolithic microsystem integration with inertial sensors and pressure sensor. Thus, we selected dry etching processes in this work, which facilitates easy fabrication handling and reduces the overall fabrication cost while limiting effects on non-exposed surfaces. The post-fabrication processing mainly involves 3 steps. In the first step, the protective In Situ Doped Poly-silicon (ISDP) material is removed from the back of the handle wafer using pure SF_6 etching gas with

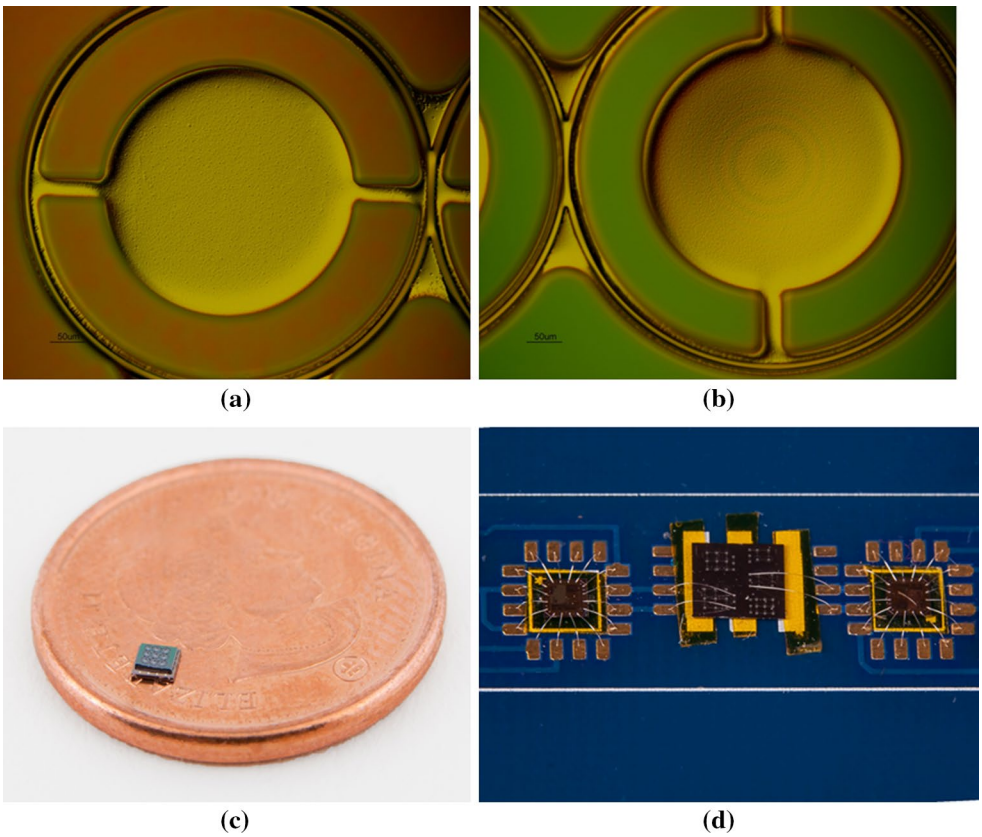

Fig. 8 Fabricated capacitive pressure sensors. **a** Bottom view with 5 µm membrane thickness, **b** bottom view with 2 µm membrane thickness, **c** relative sensor die size when placed on a Canadian 1 cent coin and **d** wire-bonding of the pressure sensor to its readout circuit

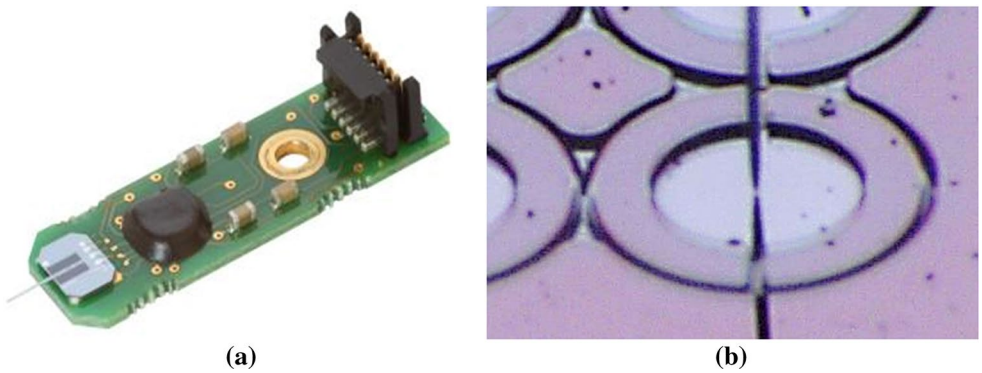

Fig. 9 Experimentation setup. **a** FemtoTools FT-S Micro-force sensing Probe. **b** Microscope image of the micromechanical testing location

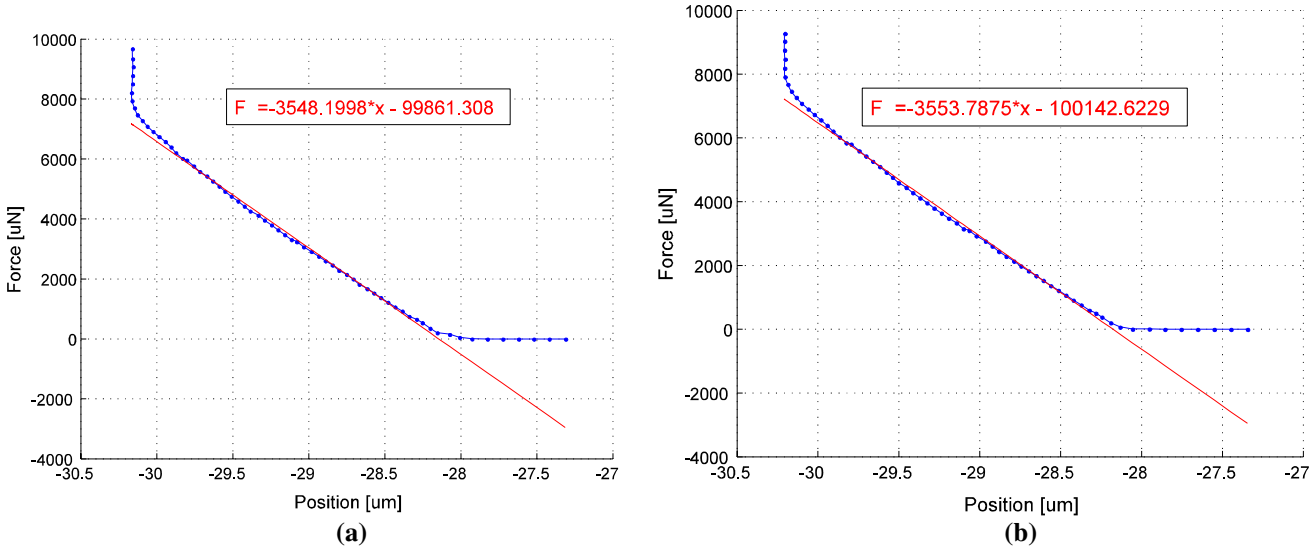

Fig. 10 Mechanical testing: experimental results showing the mechanical calibration of the sensor (**a**, **b**)

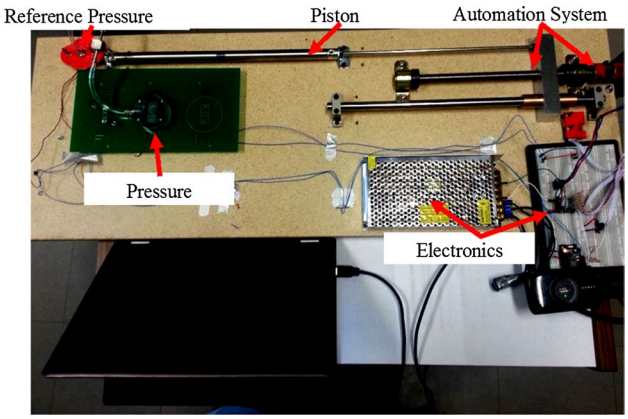

Fig. 11 Experimental Setup for the calibration of pressure sensor

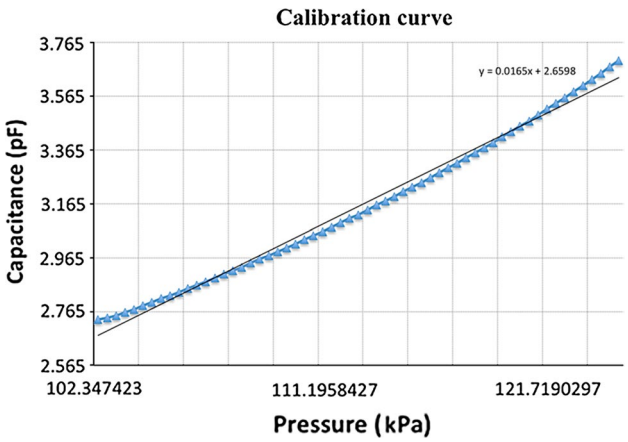

Fig. 12 Calibration curve of the pressure sensor with 5 µm membrane thickness and operating pressure range of 102–125 kPa

high physical bombarding mechanism through the use of high operating power at 1500 Watts. Here, the RF power was fixed to 50 watts to improve directionality of the bombarding species and to enhance the etch rate as well. The second step consists of completely etching-out the oxide material using CF_4 as the main etchant gas. The power used in this process is fixed to 2750 Watts with RF power of 100 Watts. The third step consists of two etching stages: the first stage is pure etching using only SF_6 with a high power of 3000 watts and 50 watts of RF power. The duration of this etching process is tuned to 1 h 30 min. However, the second etching method consists of DRIE process where SF_6 alternates with C_4F_8 following BOSCH process. The above recipe was used to precisely control the membrane thickness. This process is called the short exposure low RF power (SLEP) etch. The SLEP etch is carried out in alternating steps until the desired deflectable membrane thickness is reached. The parameters were tuned to improve surface quality and reduce the amount of material etched per step. Figure 7b represents the post-fabrication processing steps.

4 Experimental results and discussion

Figure 8 shows the optical microscope images of two sensing membranes with different thickness (5 and 2 µm) and with the same diameter of 360 µm. Using our post-fabrication processing steps, we have been able to fabricate 1 µm thick sensing membrane.

Figure 9 shows the mechanical testing setup. The sensor is placed inside the FemtoTools FT-MTA02 Micromechanical Testing and Assembly Station that includes the

micro-force sensing probe shown in Fig. 9a. This instrument allows the application of vertical force at the central position of the membrane. The FT-S micro-force probe is micro-force sensor capable of measuring forces ranging from the order of 10^{-3} to 10^{-9} N. Here, The FT-S probe has a flat silicon tip with tip size of 50 µm. The applied bias voltage and capacitance readout are used to determine the applied force and micro position of the probe (please see Fig. 9b), while bulk movements are recorded by the servomotor located in the arm holding unit.

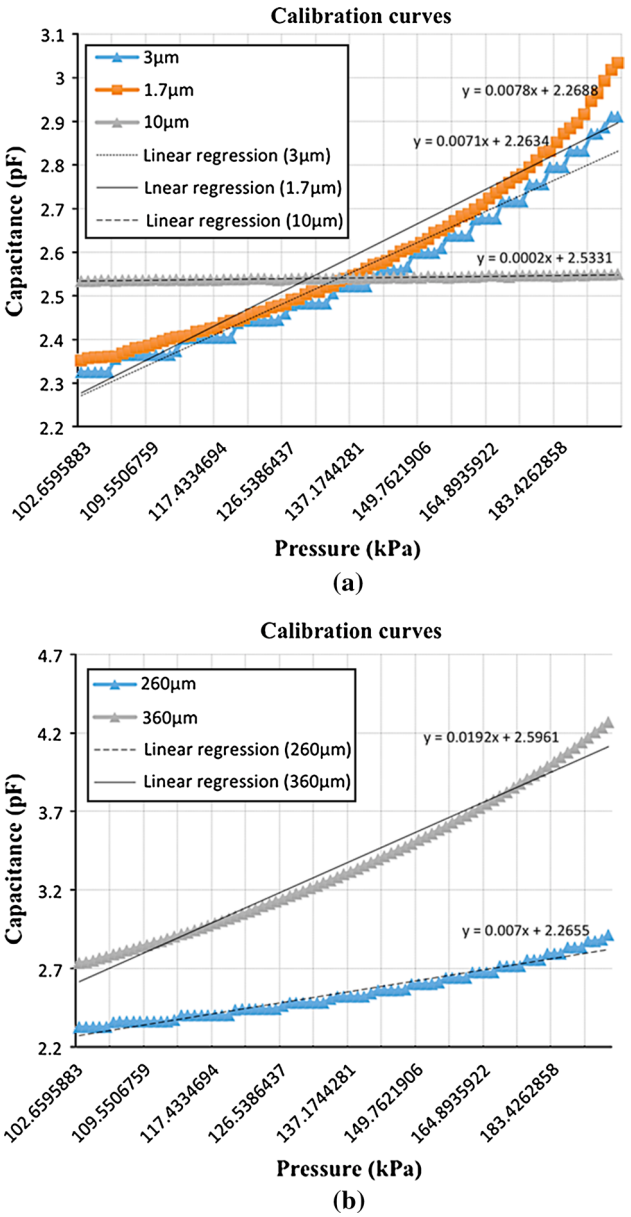

Fig. 13 Membrane Dimensions effects over the operating pressure range of 102–200 kPa. **a** The effect of varying the membrane thickness. **b** The effect of membrane diameter with fixed membrane thickness of 5 µm

Figure 10 presents the mechanical testing of the pressure sensor showing two mechanical calibration curves that includes the applied force versus the central position displacement. The experimentation are performed several times leading to a good repeatability in the measurement result with the curve slope around 3553 µN/µm or 281 µm/N. The obtained experimental results confirm well the simulation results presented in Fig. 6a (286 µm/N).

The sensor calibration is carried out by placing the pressure sensor inside a regulated pressure chamber with access to the electrical connections for interfacing with the signal conditioning circuit. The data acquisition system is based on Σ-Δ converter AD7152 that uses a combination of two signal- processing techniques, the oversampling 12-bit Σ-Δ modulator and noise shaping filter that provide a high resolution of 0.25 fF. Figure 11 shows the experimental setup used for the calibration of the pressure sensor. The testing chamber is machined out of clear Lexan and is characterized by maximum total volume of 73.4 cm^3 and full pressure range between 50 and 1200 kPa. A second piece of Lexan is placed below the Printed Circuit Board (PCB) containing the sensor die to offer more mechanical support

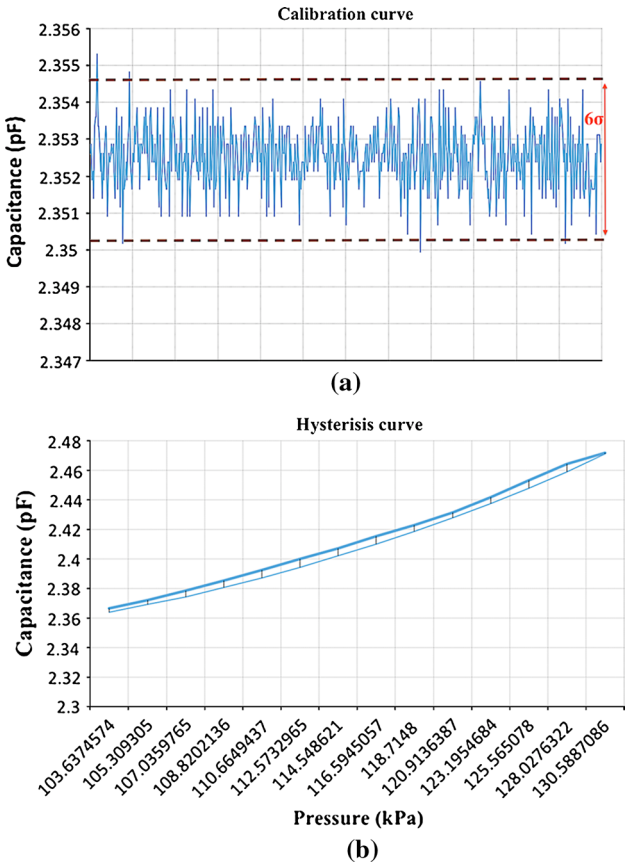

Fig. 14 Metrology performance. **a** Noise measurement with sampling time of 60 ms. **b** Maximum hysteresis deviation

at high pressures. The chamber is attached to a PCB using four bolts and an O-ring is provided to form an airtight seal. The pressure set point is controlled by automating the stroke length of the piston moving to different positions.

An absolute piezo-resistive pressure sensor from Measurement Specialties (MS5803-14BA) with an operating range of [0–14 bar] and minimum resolution of 20 Pa acts as a reference pressure sensor during the calibration testing. Figure 12 depicts the data collected from the pressure sensor of 360 μm diameter with membrane thickness of 5 μm.

The experimental results show a sensitivity of 16.5 fF/kPa with a good linearity over the current design pressure range of 102–125 kPa. The simulation results expected a sensor sensitivity of 10 fF/kPa over measurement range of 101–125 kPa. The difference between the experimental and simulation results can be explained by the microfabrication variations in the membrane dimensions. Figure 13a shows the effect of varying the thickness of the membrane while maintaining the same membrane diameter of 260 μm. The experimental data shows an inverse relationship between the sensor sensitivity and the membrane thickness over pressure range of 102–200 kPa. Figure 13b shows the results for varying the membrane diameter, 260 and 360 μm, while maintaining the same membrane thickness of 5 μm. The results indicate a linear relationship between the sensor sensitivity and the membrane diameter as previously mentioned in Sect. 2.

We performed measurements related to noise present in the pressure sensor, which has a substantial influence on the sensor resolution. There are mainly two noise sources, thermal noise that originates from the damping mechanisms in the sensor device. The other source of noise is the flicker noise (1/f noise) that arises within the signal conditioning circuit and ultimately sets the readout circuit resolution. Figure 14a illustrates an example of an output noise signal. The overall noise can be estimated from the 6σ uncertainty interval. Numerically, this parameter is equal to 0.11 fF for a given bandwidth of 32 Hz.

Hysteresis is an important parameter related to metrology performance of the pressure sensor. This parameter is deduced from the maximum deviation between sensor output at a specified value of the input signal when the input signal is increased from a low value to high value and when the input signal is decreased from a high value to a low value. Figure 14b illustrates the experimental data of pressure measurement along both increasing and decreasing the input applied pressure to the sensing membrane. The maximum deviation in the hysteresis curve is approximately 5 fF. Therefore, the total uncertainty caused by the above errors can be estimated by Eq. (5) as,

$$\sigma = \sqrt{u_{hyst}^2 + u_{noise}^2} \tag{5}$$

where, $u_{hyst} = \frac{|Y_{up} - Y_{down}|}{2\sqrt{3}}$. Thus, the sensor resolution is estimated to be 88 Pa for the current sensor operating range of 101–125 kPa. Table 1 summarizes the different parameters and specifications of the developed pressure sensor based on the obtained experimental results.

Table 1 Pressure sensor specifications and comparison to a commercial MEMS pressure sensor

Parameters	Values
Pressure range	101–125 kPa
Mechanical sensitivity	5×10^{-4} (μm/kPa)
Sensor sensitivity	16.5 fF/kPa
Resolution	88 Pa
Diameter	360 μm
Membrane thickness	5 μm
Unit number	4
Dimension area	750×750 (μm^2)

5 Conclusions

We reported, for the first time, the design and fabrication of a MEMS absolute pressure sensor using a modified commercial MEMS process that provides wafer level vacuum encapsulation. The MIDIS process used for the development of the pressure sensor provides the ability to monolithically integrate inertial sensors with pressure sensors toward multi-DOF inertial measurement units. The developed absolute capacitive pressure sensor provided high performance specifications including good linearity, sensitivity and stability, low power consumption, and good repeatability and reproducibility. Our approach of using a standard MEMS process to develop MEMS sensors provides a promising option allowing highly efficient and reproducible manufacturing at large volumes, lower cost, and high yields. The Through Silicon Vias (TSVs) available with the developed pressure sensor provides excellent benefits in terms of reducing the overall product cost, simplifying packaging constraints, and easing supply-chain logistics.

Acknowledgments We would like to acknowledge the financial support given by Natural Sciences and Engineering Research Council of Canada (NSERC) and Canadian Institutes of Health Research through the Collaborative Health Research Projects and University of Dayton, OH. We would like to acknowledge the support from Canada Microelectronics Corporations in providing access to the MIDIS fabrication process from TDSI.

References

Barlian AA, Park WT, Mallon JR, Rastegar AJ, Pruitt BL (2009) Review: semiconductor piezoresistance for microsystems. Proc IEEE 97:513–552

Bryzek J, Roundy S, Bircumshaw B, Chung C, Castellino K, Stetter JR et al (2006) Marvelous MEMS. Circuits Devices Mag IEEE 22:8–28

Chan WP, Narducci M, Gao Y, Cheng MY, Cheong JH, George AK et al (2014) A monolithically integrated pressure/oxygen/temperature sensing SoC for multimodality intracranial neuromonitoring. IEEE J Solid-State Circuits 49:2449–2461

Chavan AV, Wise KD (2001) Batch-processed vacuum-sealed capacitive pressure sensors. J Microelectromech Syst 10:580–588

Chiou JC, Huang YC, Yeh GT (2016) A capacitor-based sensor and a contact lens sensing system for intraocular pressure monitoring. J Micromech Microeng 26(1)

Chitnis G, Maleki T, Samuels B, Cantor LB (2013) A minimally invasive implantable wireless pressure sensor for continuous IOP monitoring. IEEE Trans Biomed Eng 60:250–256

Choa SH (2005) Reliability of vacuum packaged MEMS gyroscopes. Microelectron Reliab 45:361–369

DeHennis A, Chae J (2008) Pressure sensors. In: Comprehensive microsystems, vol 2. Elsevier, pp 101–133

Eaton WP, Smith JH (1997) Micromachined pressure sensors: review and recent developments. Smart Mater Struct 6:529–539

Esashi M (2008) Wafer level packaging of MEMS. J Micromech Microeng 18(7)

Fleming WJ (2001) Overview of automotive sensors. Sens J IEEE 1:296–308

Guckel H, Burns DW, Tilmans HAC, DeRoo DW (1988) Mechanical properties of fine grained polysilicon-the repeatability issue, presented at the Solid-State Sensor and Actuator Workshop, 1988. Technical Digest., IEEE, Hilton Head Island, SC, USA

Hsu YP, Young DJ (2014) Skin-coupled personal wearable ambulatory pulse wave velocity monitoring system using microelectromechanical sensors. IEEE Sens J 14:3490–3497

Jones TB, Nenadic NG (2013) Practical MEMS devices. In: Electromechanics and MEMS. Cambridge University Press, p 577

Kaajakari V (2009) Practical MEMS: design of microsystems, accelerometers, gyroscopes, RF MEMS, optical MEMS, and microfluidic systems. Small Gear Publishing, Las Vegas

Leclerc J (2007) MEMs for aerospace navigation. IEEE Aerosp Electron Syst Mag 22:31–36

Lee TJ, Zihajehzadeh S, Loh D, Hoskinson R, Park EJ (2015) Automatic jump detection in skiing/snowboarding using head-mounted MEMS inertial and pressure sensors. Proc Inst Mech Eng Part P J Sports Eng Technol 229:278–287

Merdassi A, Kezzo MN, Xereas G, Chodavarapu VP (2015a) Wafer level vacuum encapsulated tri-axial accelerometer with low cross-axis sensitivity in a commercial MEMS Process. Sensors Actuators a-Phys 236:25–37

Merdassi A, Yang P, Chodavarapu VP (2015b) A wafer level vacuum encapsulated capacitive accelerometer fabricated in an unmodified commercial. MEMS Process Sens 15:7349–7359

Mounier CTE, Girardin G (2015) MEMS markets: status of the MEMS Industry 2015. http://www.slideshare.net/Yole_Developpement/status-of-thememsindustry2015sample

PRNewswire (2015) http://www.prnewswire.com/news-releases/global-mems-pressure-sensors-market-2015-2019-300023028.html. Accessed 16 June 2016

Saejok K, Phinyo B, Chaowicharat E, Ratanaudomphisut E (2008) Effect of temperature to characteristics of polysilicon based surface micromachining piezoresistive pressure sensor, presented at the Electrical Engineering/Electronics, Computer, Telecommunications and Information Technology, 2008. ECTI-CON 2008. 5th International Conference on Krabi

Sharma M, Sarraf EH, Baskaran R, Cretu E (2012) Parametric resonance: amplification and damping in MEMS gyroscopes. Sens Actuators a-Phys 177:79–86

Stone R, Gardien F, Filipe A, Pisella C, Roggi A, Boillot FO-X (2010) Miniature implantable pressure sensors for medical applications. J Med Devices 4:027507-027507

Tadigadapa S, Mateti K (2009) Piezoelectric MEMS sensors: state-of-the-art and perspectives. Meas Sci Technol 20(9)

Wise KD (2007) Integrated sensors, MEMS, and microsystems: reflections on a fantastic voyage. Sens Actuators a-Phys 136:39–50

Xereas G, Chodavarapu VP (2015) Wafer-level vacuum-encapsulated lame mode resonator with f-Q product of 2.23 × 10(13) Hz. IEEE Electron Device Lett 36:1079–1081